

Silver-epoxy microwave filters and thermalizers for millikelvin experiments

Christian P. Scheller,¹ Sarah Heizmann,¹ Kristine Bedner,¹ Dominic Giss,¹ Matthias Meschke,² Dominik M. Zumbühl,^{1,a)} Jeremy D. Zimmerman,³ and Arthur C. Gossard³

¹Department of Physics, University of Basel, Klingelbergstrasse 82, CH-4056 Basel, Switzerland

²Low Temperature Laboratory, Aalto University, School of Science, 00076 Aalto, Finland

³Materials Department, University of California, Santa Barbara, California 93106, USA

(Received 24 March 2014; accepted 13 May 2014; published online 29 May 2014)

We present silver-epoxy filters combining excellent microwave attenuation with efficient wire thermalization, suitable for low temperature quantum transport experiments. Upon minimizing parasitic capacitances, the attenuation reaches ≥ 100 dB above ≈ 150 MHz and—when capacitors are added—already above ≈ 30 MHz. We measure the device electron temperature with a GaAs quantum dot and demonstrate excellent filter performance. Upon improving the sample holder and adding a second filtering stage, we obtain electron temperatures as low as 7.5 ± 0.2 mK in metallic Coulomb blockade thermometers. © 2014 Author(s). All article content, except where otherwise noted, is licensed under a Creative Commons Attribution 3.0 Unported License.

[<http://dx.doi.org/10.1063/1.4880099>]

Advancing to lower system temperatures is of fundamental interest, allowing to resolve smaller energy scales and hence opening the door for new physics. Examples include fractional quantum hall states,^{1–4} nuclear spin phase transitions,^{5–8} and many more. Dilution refrigerators with base temperatures as low as 5 mK are readily available, but typical electron temperatures T_e in semiconductor nanoscale devices are often considerably higher. This is due to insufficient thermalization, absence of adequate filtering of high frequency radiation^{9,10} as well as low frequency noise from the measurement setup including ground loops.

To attenuate microwave radiation, various types of cryogenic filters have been developed, such as metal powder filters,^{11–14} micro fabricated filters,^{15–18} thermo-coax cables,^{19,20} copper tapeworm filters,^{21,22} thin film filters,²³ and lossy transmission lines.²⁴ An overview of various microwave filters is given in Ref. 25. Despite decades of research, the state of the art is not satisfactory for cooling at 10 mK to below. Besides filtering strategies, reduction of internal heat leaks and proper thermalization for sample, sample holder and wires are equally important. We note that the electron-phonon coupling has a very strong temperature dependence,^{2,26} scaling as T^5 , making low temperature cooling very challenging. Wiedemann-Franz cooling²⁶ through the electrical sample wires scales much more favorably, as T^2 , and eventually becomes the dominant cooling mechanism.²

In this Letter, we present Ag-epoxy cryogenic filters uniting excellent microwave attenuation with efficient thermalization, suitable for low temperature electronic measurements. The filters are modular, of small size, robust against thermal cycling, and possess a predictable attenuation spectrum which can be understood as a skin-effect filter in a lossy transmission line model. Thermometry experiments using a GaAs quantum dot and metallic Coulomb blockade thermometers (CBTs) are employed to investigate the filter

performance, demonstrating CBT electron temperatures²⁷ down to 7.5 ± 0.2 mK.

The filters are made by neatly winding 2.5 m of insulated Cu-wire (diameter $D = 0.1$ mm) with a magnet winding machine around a precast Ag-epoxy²⁸ rod to form a 5-layer coil. While winding, we continuously wet the rod and wires with Ag-epoxy to embed the wire in a conducting matrix, ensuring full electrical encapsulation and good thermal contact of the wire throughout the filter. Standard micro coaxial connectors are soldered and, after gluing parts together with insulating epoxy,²⁹ a high-conductivity Cu-braid is fastened to the filter also with Ag-epoxy, serving as a thermal anchor. A completed filter is shown in Fig. 1 (inset). We mount the filters at the mixing chamber (MC) of a dilution refrigerator with $T_{MC} \approx 5$ mK, at base temperature. We emphasize that the wire is tightly embraced in the Ag-epoxy matrix, which is a good

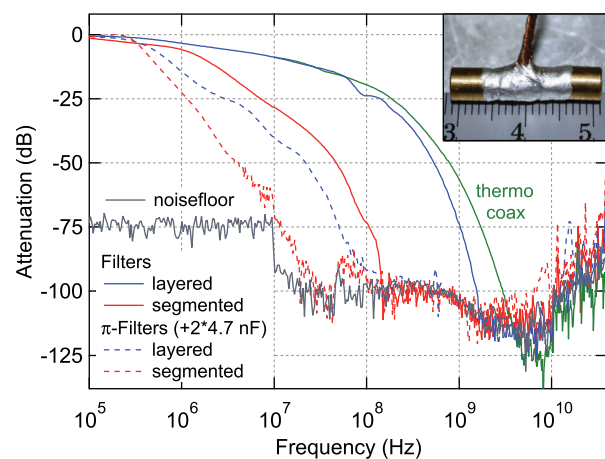


FIG. 1. Attenuation of thermo-coax and various filters at room temperature. Blue and red represent layered and segmented filters, respectively, with DC resistance $\approx 5 \Omega$ (< 50 m Ω at 4.2 K) and capacitance ≈ 4 nF. The dashed curves are from π -type filters with 4.7 nF added at each end. The jump in the noise floor at 10 MHz is due to use of a different analyzer at frequencies ≥ 10 MHz. Cooling to 4.2 K does not significantly alter the attenuation. Inset: photo of a filter (22 mm long, 5 mm diameter) with centimeter scale bar.

^{a)}Electronic mail: dominik.zumbuhl@unibas.ch

electrical conductor down to the lowest T_{MC} . This is facilitating both cooling of the wire through the $d_{ins.} \sim 8 \mu\text{m}$ thick polyurethane insulation as well as high frequency filtering—thus presenting an advantage over earlier designs.

The attenuation profile is shown in Fig. 1, providing an attenuation ≥ 100 dB above 1.5 GHz (solid blue trace). Parasitic or stray capacitances can severely degrade the high-frequency attenuation. An optimized filter layout can reduce such capacitances: we split-up the coil into separate smaller segments arranged in series, resulting in a segmented filter, as opposed to the layered filter previously described. For layered filters, the first and the last layers of the coil are relatively close, separated only by 3 layers of Cu-wire or equivalently 0.3 mm distance. In contrast, the first and last coils are at a distance of ≈ 5 mm for the segmented filters. In a naive plate capacitor model, this corresponds to a reduction of capacitive coupling by a factor of ~ 10 . Indeed, we obtain 100 dB or more already above 150 MHz for the segmented filters (red solid trace, Fig. 1), at 10 times lower frequencies compared to the layered filter.

The filter attenuation can be modeled as a lossy, distributed transmission line with skin-effect: the resistance per length R_{IC} and R_{OC} of inner and outer conductor, respectively, depend on frequency. While DC-currents are supported by the whole cross section $A = \pi D^2/4$ of the Cu-wire with diameter D , the skin effect forces AC-currents at frequency ν to an annulus of width $\delta = 1/\sqrt{\sigma_{Cu}\mu_{Cu}\nu\pi}$ —the skin depth. Here, σ_{Cu} denotes the conductivity and μ_{Cu} the magnetic permeability of the Cu-wire. The effective cross section therefore reduces to $A = D\pi\delta$, and consequently R_{IC} increases as a function of ν . Equivalent arguments hold for the outer conductor. Note that due to its smaller conductivity $\sigma_{epoxy} \ll \sigma_{Cu}$, the Ag-epoxy outer conductor is dominating the total resistance $R_{tot}(\nu) = R_{IC}(\nu) + R_{OC}(\nu)$ at high $\nu \geq 2$ MHz.

The resulting attenuation is $\propto -\nu^{3/4}$ for low frequencies $2\pi\nu L \ll R_{tot}(\nu)$ and $\propto -\nu^{1/2}$ for high frequencies in the GHz regime with a smooth transition in between. Here, $L = \mu_0/2\pi \ln((D + 2d_{ins.})/D)$ denotes the inductance per length. For a single layer filter, where additional parasitic capacitances not included in the theory are negligible, the model is in very good agreement with the measured attenuation without using any fit parameters, see supplementary material³⁰ for details. This demonstrates the validity of the skin-effect lossy transmission line model and can explain the general functional shape of the measured filter attenuation curves. When comparing the model with the segmented and layered filters described above, the agreement between theory and measured attenuation is still good once a fit parameter is allowed, e.g., the capacitance per length.

A π -type filter can be created by adding capacitors³¹ to both filter ends, further increasing the attenuation.¹⁴ Both layered and segmented π -filters are shown in Fig. 1 as dashed curves, delivering an attenuation ≥ 100 dB attenuation already above 30 MHz for segmented π -type filter. However, in order not to reduce the bandwidth for future experiments too much and because of increased current preamplifier noise with large capacitances, the segmented filters without additional capacitors were chosen for the electron temperature measurements. Further, we note that replacing the central

rod with a mixture of insulating epoxy²⁹ and Fe powder¹⁴ or replacing the copper wire with resistive wire did not improve the filter performance. Once properly completed, repeated thermal cycling has not yet caused failure of any of the over hundred filters in use in our laboratory.

We now turn to the filter performance measured by the device electron temperature T_e with a GaAs quantum dot thermometer,^{32–40} comparing T_e with and without filters. For all measurements below, the sample wires are connected to the room temperature measurement setup through ~ 1.5 m long thermo-coax cables,⁴¹ which are very effective attenuators above a few GHz, see green curve in Fig. 1, up to very high frequencies ≈ 1 THz.¹⁹ The Ag-epoxy filters provide additional thermalization and serve to significantly bring down the low-pass cut-off frequency of the combined thermo-coax and Ag-epoxy filter system.

We use a surface gated GaAs/AlGaAs quantum dot (see Fig. 2, lower inset) in the temperature broadened Coulomb blockade regime as an electron thermometer, probing the Fermi-Dirac distribution of the reservoirs. Gates N, L, R and P isolate the quantum dot from the surrounding 2D gas, while source (S) and drain (D) ohmic contacts serve for current injection and detection. Details on sample fabrication are given in Ref. 42. All measurements presented here were performed in the single electron regime. The dot differential conductance g at zero DC-bias peaks whenever one of its energy levels is aligned with the chemical potential of source and drain, see upper inset, Fig. 2. The shape and width ΔV_G in gate voltage of this peak reflects the reservoir temperatures and provides a primary electron thermometer^{32–34} in the limit of small tunnel rates to source and drain (and large dot level spacing) compared to temperature. The conversion between measured peak width ΔV_G and energy ΔE is done by means of the lever arm α , $\Delta E = \alpha \Delta V_G$. To determine α , a DC-bias $eV_{SD} \gg k_B T_e$ is applied (Boltzmann constant k_B and

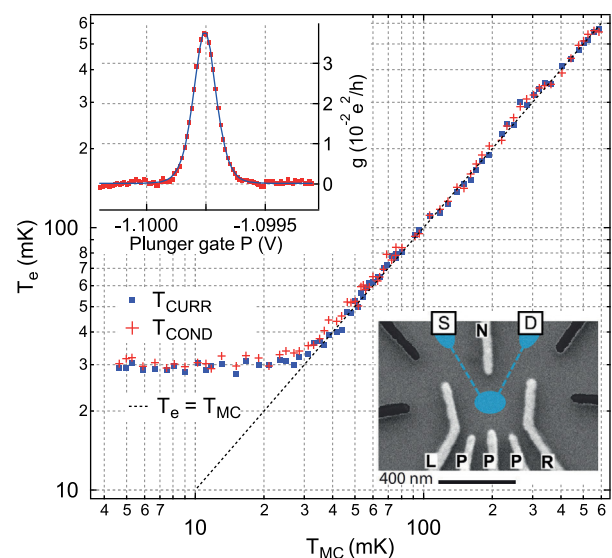


FIG. 2. Electron temperature T_e extracted from GaAs dot current and conductance measurements as indicated versus refrigerator temperature T_{MC} , with dashed line showing ideal thermalization $T_e = T_{MC}$. The upper inset shows a typical zero-bias peak at base temperature with \cosh^{-2} fit.³³ Lower inset: micrograph of a similar device. Gates N, L, R, and P (light grey) form the dot. Dark gates are grounded.

electron charge $e > 0$), splitting the zero-bias conductance peak into two peaks with gate-voltage separation V_{sep} and giving $\alpha = eV_{\text{SD}}/V_{\text{sep}}$. All conductance data are recorded with a standard lock-in technique using an AC-excitation experimentally chosen sufficiently small to avoid heating ($2 \mu\text{V}$ at base temperature).

Instead of differential conductance g at $V_{\text{SD}} = 0$, we can also measure the DC dot current I_{DC} at large bias $eV_{\text{SD}} \gg k_B T$, which shows transitions between low and high current when a dot level is crossing the chemical potential of source and drain. These current transitions reflect the Fermi-Dirac distribution of the corresponding reservoir and allow extraction of source and drain temperature separately (see Ref. 40 for details). Here, α is simply given by the ratio of the applied bias V_{SD} , divided by the separation of the inflection points for the two distributions. We stress that I_{DC} is determined by the tunneling rates and does not depend on the applied DC voltage as long as excited states (and cotunneling) do not contribute, as we assume here. Also, reducing the DC bias did not affect T_e . Further, there is no systematic deviation between source and drain temperatures, and we conclude that energetic electrons at $\geq 100 \mu\text{eV}$ become efficiently thermalized in the reservoirs.

Fig. 2 displays the extracted electron temperatures from the same warmup using both g and I_{DC} . We measure the zero-bias g -peak with a finite AC excitation V_{AC} and then the I_{DC} steps at finite V_{SD} , and repeat this cycle. We perform Fermi-Dirac distribution fits on the I_{DC} steps, forcing the two reservoir temperatures to be identical in order to obtain more reliable fitting results and obtain the reservoir electron temperature T_{CURR} as well as the lever arm α . Finally, we get the reservoir electron temperature T_{COND} from \cosh^{-2} fits^{32–34} to the g -peak using the same lever arm. We note that for the g measurements, already a small $eV_{\text{DC}} \sim k_B T$ results in a broadened peak and an overestimation of T_{COND} . Therefore, a feedback mechanism was implemented that compensates any V_{SD} drift by minimizing I_{DC} in the zero-bias measurement, therefore ensuring excellent alignment of source and drain during the ~ 40 h measurement shown in Fig. 2.

Both electron temperatures T_{CURR} and T_{COND} agree well with each other over the whole temperature range and, above 40 mK, also with T_{MC} , measured with a RuO_2 thermometer, thus demonstrating excellent thermometer operation. The RuO_2 thermometer was precalibrated with a fixed point device and agrees very well with a Cerium Magnesium Nitrate paramagnetic inductance thermometer.²⁶ Below 40 mK, T_e starts deviating from T_{MC} and saturates at ~ 30 mK. Upon reducing electronic noise and simplifying the measurement setup (measuring only I_{DC}), the electron temperature T_e is reduced down to $T_{\text{CURR}} = 18 \pm 3$ mK, obtained from an average over several traces. An example of such a trace including Fermi-Dirac fits of the current steps and individually extracted source/drain temperatures is presented in the upper panel of Fig. 3.

When the filters are removed (replaced with plain adaptors) without changing any other part of the experiment, the electron temperature increases to $T_{\text{CURR}} \approx 75$ mK, see lower panel of Fig. 3, clearly demonstrating the efficiency of the filters. Note that due to the elevated electron temperature, more DC bias is applied to better separate the source and drain current steps. However, this does not increase the

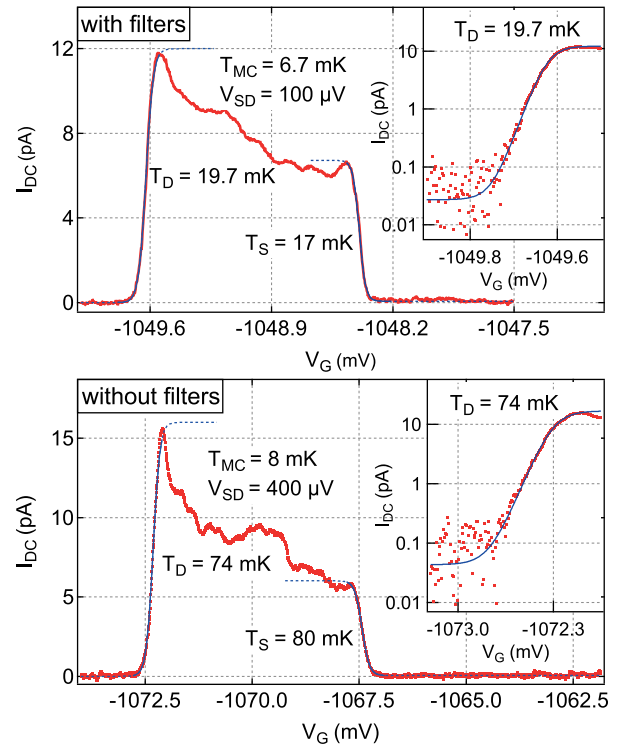


FIG. 3. DC current I_{DC} through the GaAs dot as a function of plunger gate voltage V_G taken at base temperature, with individual Fermi-Dirac fits for source and drain leads, as indicated, comparing data with filters (upper panel) and without filters (lower panel). The insets show the same data and fit in log-scale for the drain side. The linear current increase seen here clearly indicates the temperature broadened regime.

electron temperature, as discussed already earlier (also here, smaller bias was tested).

There is still room for further improving the electron temperature, considering that the refrigerator cools to $T_{\text{MC}} = 5$ mK. An additional miniaturized Ag-epoxy filtering/thermalization stage is placed directly inside the Faraday cup, i.e., inside the shielded sample can. Furthermore, a heat sunk sample holder made from conductive Ag-epoxy is used, and the ceramic chip carrier (known to suffer from heat release) is replaced with a standard plastic dip socket equipped with a 1 mm thick gold plated and heat sunk copper backplane. We proceed to measure electron temperatures with this improved two stage filtering/thermalization setup. For simplicity, metallic CBTs are used that—in contrast to GaAs dots—do not require gate tuning to deliver the device electron temperature. We note that CBTs have cooled to very similar electron temperatures as the dot before improving the setup.

The CBTs consist of 7 parallel arrays with 64 angle evaporated tunnel junctions between metal islands,^{43,44} operating in the regime where the charging energy E_C is comparable to temperature⁴⁵ (in contrast to the dot measurements in Figs. 2 and 3, where $E_C \gg k_B T_e$). The full width at half minimum of the V_{SD} dependent conductance dip (see inset of Fig. 4) can serve as a primary thermometer.^{46,47} Here, however, we use the conductance dip $\Delta g/g$ as a secondary thermometer to avoid heating at finite bias.²⁷ At high temperatures, where the CBTs are in thermal equilibrium with the refrigerator, E_C can be extracted from the temperature dependent $\Delta g/g$ using the relation⁴⁵ $\Delta g/g = u/6 - u^2/60 + u^3/630$, where $u = E_C/k_B T_{\text{CBT}}$.

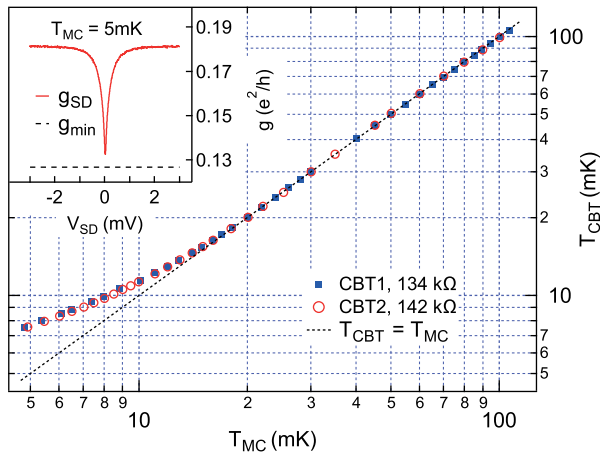


FIG. 4. CBT electron temperature T_{CBT} versus mixing chamber temperature T_{MC} for two CBTs on the same wafer, measured in a perpendicular magnetic field of 250 mT to drive the Al normal. Ideal thermalization $T_{\text{CBT}} = T_{\text{MC}}$ is indicated as a dashed line. The inset shows g as a function of V_{SD} at base temperature (red), exhibiting a zero-bias conductance dip. The minimum conductance g_{min} , measured while waiting at $V_{\text{SD}} = 0$ for an extended time, is indicated as dashed line—well below $g(V_{\text{SD}} = 0)$ when sweeping.

With E_{C} obtained in this way, the measured $\Delta g/g$ can be converted to the corresponding electron temperature T_{CBT} in the full temperature range.

Fig. 4 shows T_{CBT} as a function of refrigerator temperature T_{MC} for two CBTs, measured using standard lock-in technique with AC excitation of $4 \mu\text{V}$ (experimentally chosen small enough to avoid heating effects). At the lowest temperatures, the zero-bias conductance $g(V_{\text{SD}} = 0)$ drops over a time span of several minutes and eventually saturates at a value g_{min} , clearly lower than the minimum conductance from V_{SD} sweeps, see inset of Fig. 4. We therefore use g_{min} in order to obtain the conductance dip $\Delta g/g$ and consequently the electron temperature T_{CBT} . The extracted electron temperatures T_{CBT} from both devices (circles and squares) agree very well with each other and with the refrigerator temperature T_{MC} down to about 15 mK, where the electron temperatures begin to saturate, eventually reaching a minimum²⁷ $T_{\text{CBT}} = 7.5 \pm 0.2$ mK for $T_{\text{MC}} \approx 5$ mK.

We note that fitting the data in Fig. 4 with a power law²⁷ $T_{\text{CBT}}^p = T_{\text{S}}^p + T_{\text{MC}}^p$ gives $p = 2.7 \pm 0.2$ and $T_{\text{S}} = 6.9 \pm 0.1$ mK, where T_{S} is a theoretical $T_{\text{MC}} = 0$ K saturation limit of T_{CBT} . This exponent p is clearly lower than $p = 5$ which corresponds to electron-phonon coupling,²⁶ thus indicating an additional cooling mechanism stronger than electron-phonon cooling at low temperatures, presumably electronic (i.e., Wiedemann-Franz²⁶) cooling.²⁷ Nevertheless, if only electron-phonon coupling is assumed, the lowest electron temperature reached corresponds to a residual heat leak of 13 aW per junction.^{27,43}

In conclusion, we have presented miniature microwave filters uniting superior attenuation with efficient wire thermalization. The attenuation reaches ≥ 100 dB above 150 MHz or, when capacitors are added, already above 30 MHz. The filters are modular, of small size, robust against thermal cycling, and the attenuation is well understood by skin-effect filtering in a lossy transmission line model. Combined with thermo-coaxes, one stage of Ag-epoxy filters reduces the electron temperature, measured with a GaAs quantum dot, from

≈ 75 mK down to ≈ 18 mK. With an improved setup comprising, a second Ag-epoxy filtering stage and a better chip holder, electron temperatures as low as 7.5 ± 0.2 mK are obtained in metallic CBTs.

Further experiments are required to determine whether the second filter stage or the improved chip carrier (or both) are necessary for the improvement from 18 mK to 7.5 mK. Finally, we point out that the filtering strategy introduced here was recently used to find evidence for helical nuclear spin order in GaAs quantum wires⁸—thus showing that the extensive filtering and thermalization introduced here can be important for studying new physics.

We thank J. P. Pekola for his support and G. Frossati, M. Steinacher, and A. de Waard for valuable inputs on the filter design. This work was supported by the Swiss Nanoscience Institute (SNI), NCCR QSIT, Swiss NSF, ERC starting grant, and EU-FP7 SOLID and MICROKELVIN.

- ¹R. Willett, J. P. Eisenstein, H. L. Stormer, D. C. Tsui, A. C. Gossard, and J. H. English, *Phys. Rev. Lett.* **59**, 1776 (1987).
- ²W. Pan, J. S. Xia, V. Shvarts, D. E. Adams, and H. L. Stormer, *Phys. Rev. Lett.* **83**, 3530 (1999).
- ³I. P. Radu, J. B. Miller, C. M. Marcus, M. A. Kastner, L. N. Pfeiffer, and K. W. West, *Science* **320**, 899 (2008).
- ⁴M. Dolev, M. Heiblum, V. Umansky, A. Stern, and D. Mahalu, *Nature* **452**, 829 (2008).
- ⁵P. Simon, B. Braunecker, and D. Loss, *Phys. Rev. B* **77**, 045108 (2008).
- ⁶B. Braunecker, P. Simon, and D. Loss, *Phys. Rev. Lett.* **102**, 116403 (2009).
- ⁷B. Braunecker, P. Simon, and D. Loss, *Phys. Rev. B* **80**, 165119 (2009).
- ⁸C. P. Scheller, T.-M. Liu, G. Barak, A. Yacoby, L. N. Pfeiffer, K. W. West, and D. M. Zumbühl, *Phys. Rev. Lett.* **112**, 066801 (2014).
- ⁹J. M. Hergenrother, J. G. Lu, M. T. Tuominen, D. C. Ralph, and M. Tinkham, *Phys. Rev. B* **51**, 9407 (1995).
- ¹⁰J. P. Pekola, V. F. Maisi, S. Kafanov, N. Chekurov, A. Kemppinen, Y. A. Pashkin, O. P. Saira, M. Möttönen, and J. S. Tsai, *Phys. Rev. Lett.* **105**, 026803 (2010).
- ¹¹J. M. Martinis, M. H. Devoret, and J. Clarke, *Phys. Rev. B* **35**, 4682 (1987).
- ¹²A. Fukushima, A. Sato, A. Iwasa, Y. Nakamura, T. Komatsuzaki, and Y. Sakamoto, *IEEE Trans. Instrum. Meas.* **46**, 289 (1997).
- ¹³F. P. Milliken, J. R. Rozen, G. A. Keefe, and R. H. Koch, *Rev. Sci. Instrum.* **78**, 024701 (2007).
- ¹⁴A. Lukashenko and A. Ustinov, *Rev. Sci. Instrum.* **79**, 014701 (2008).
- ¹⁵D. Vion, P. F. Orfila, P. Joyez, D. Esteve, and M. H. Devoret, *J. Appl. Phys.* **77**, 2519 (1995).
- ¹⁶H. Courtois, O. Buisson, J. Chaussy, and B. Pannetier, *Rev. Sci. Instrum.* **66**, 3465 (1995).
- ¹⁷H. le Sueur and P. Joyez, *Rev. Sci. Instrum.* **77**, 115102 (2006).
- ¹⁸L. Longobardi, D. A. Bennett, V. Patel, W. Chen, and J. E. Lukens, *Rev. Sci. Instrum.* **84**, 014706 (2013).
- ¹⁹A. B. Zorin, *Rev. Sci. Instrum.* **66**, 4296 (1995).
- ²⁰D. C. Glatli, P. Jacques, A. Kumar, P. Pari, and L. Saminadayar, *J. Appl. Phys.* **81**, 7350 (1997).
- ²¹L. Spietz, J. Teufel, and R. J. Schoelkopf, “A Twisted Pair Cryogenic Filter,” e-print [arXiv:cond-mat/0601316v1](https://arxiv.org/abs/cond-mat/0601316v1) (2006).
- ²²H. Bluhm and A. Moler, *Rev. Sci. Instrum.* **79**, 014703 (2008).
- ²³I. Jin, A. Amar, and F. C. Wellstood, *Appl. Phys. Lett.* **70**, 2186 (1997).
- ²⁴D. H. Slichter, O. Naaman, and I. Siddiqi, *Appl. Phys. Lett.* **94**, 192508 (2009).
- ²⁵K. Bladh, D. Gunnarsson, E. Hürfeld, S. Devi, C. Kristoffersson, B. Smålander, S. Pehrson, T. Claeson, P. Delsing, and M. Taslakov, *Rev. Sci. Instrum.* **74**, 1323 (2003).
- ²⁶F. Pobell, *Matter and Methods at Low Temperatures* (Springer, Berlin, 1992).
- ²⁷L. Casparis, M. Meschke, D. Maradan, A. C. Clark, C. P. Scheller, K. K. Schwarzwälder, J. P. Pekola, and D. M. Zumbühl, *Rev. Sci. Instrum.* **83**, 083903 (2012).
- ²⁸Silver epoxy E4110, available at EPO-TEK.

- ²⁹Emerson and Cuming Stycast 2850FT black epoxy.
- ³⁰See supplementary material at <http://dx.doi.org/10.1063/1.4880099> for a detailed description of the skin-effect filtering in a lossy transmission line model.
- ³¹Discoidal ceramic capacitors with negligible temperature dependence, Pacific Aerospace and Electronics.
- ³²M. A. Kastner, *Rev. Mod. Phys.* **64**, 849 (1992).
- ³³H. van Houten, C. W. J. Beenakker, and A. A. M. Staring, "Coulomb blockade oscillations in semiconductor nanostructures," in *Single Charge Tunneling, NATO ASI Series* Vol. 294, edited by H. Grabert and M. H. Devoret (Springer, New York, 1992).
- ³⁴L. P. Kouwenhoven, C. M. Marcus, P. L. McEuen, S. Tarucha, R. M. Westervelt, and N. S. Wingreen, "Electron transport in quantum dots," in *Proceedings of the NATO Advanced Study Institute on Mesoscopic Electron Transport* (Springer, Dordrecht, Netherlands, 1996), Vol. 45, pp. 105–214.
- ³⁵I. Karakurt, V. J. Goldman, J. Liu, and A. Zaslavsky, *Phys. Rev. Lett.* **87**, 146801 (2001).
- ³⁶R. M. Potok, I. G. Rau, H. Shtrikman, Y. Oreg, and D. Goldhaber-Gordon, *Nature* **446**, 167 (2007).
- ³⁷A. Rossi, T. Ferrus, and D. A. Williams, *Appl. Phys. Lett.* **100**, 133503 (2012).
- ³⁸A. Mavalankar, S. J. Chorley, J. Griffiths, G. A. C. Jones, I. Farrer, D. A. Ritchie, and C. G. Smith, *Appl. Phys. Lett.* **103**, 133116 (2013).
- ³⁹P. Torresani, M. J. Martínez-Pérez, S. Gasparinetti, J. Renard, G. Biasiol, L. Sorba, F. Giazotto, and S. D. Franceschi, *Phys. Rev. B* **88**, 245304 (2013).
- ⁴⁰D. Maradan, L. Casparis, T.-M. Liu, D. E. F. Biesinger, C. P. Scheller, D. M. Zumbühl, J. Zimmerman, and A. C. Gossard, *J. Low Temp. Phys.* **175**, 784 (2014).
- ⁴¹Heating element 1NcAc, 0.5 mm diameter, from Thermocoax SA, heat sunk at 4.2 K, at the 1 K pot, at the 50 mK plate, and the MC-plate.
- ⁴²D. M. Zumbühl, C. M. Marcus, M. P. Hanson, and A. C. Gossard, *Phys. Rev. Lett.* **96**, 206802 (2006).
- ⁴³M. Meschke, J. P. Pekola, F. Gay, R. E. Rapp, and H. Godfrin, *J. Low Temp. Phys.* **134**, 1119 (2004).
- ⁴⁴J. P. Pekola, K. P. Hirvi, J. P. Kauppinen, and M. A. Paalanen, *Phys. Rev. Lett.* **73**, 2903 (1994).
- ⁴⁵A. V. Feshchenko, M. Meschke, D. Gunnarsson, M. Prunnila, L. Roschier, J. S. Penttilä, and J. P. Pekola, *J. Low Temp. Phys.* **173**, 36 (2013).
- ⁴⁶S. Farhangfar, K. P. Hirvi, J. P. Kauppinen, J. P. Pekola, J. J. Toppari, D. V. Averin, and A. N. Korotkov, *J. Low Temp. Phys.* **108**, 191 (1997).
- ⁴⁷M. Meschke, J. Engert, D. Heyer, and J. P. Pekola, *Int. J. Thermophys.* **32**, 1378 (2011).

Supplementary Information

Silver-Epoxy Microwave Filters and Thermalizers for Millikelvin Experiments

Christian P. Scheller,¹ Sarah Heizmann,¹ Kristine Bedner,¹ Dominic Giss,¹ Matthias Meschke,² Dominik M. Zumbühl,^{1, a)} Jeramy D. Zimmerman,³ and Arthur C. Gossard³

¹⁾ *University of Basel, Klingelbergstrasse 82, CH-4056 Basel, Switzerland*

²⁾ *Low Temperature Lab, Aalto University, School of Science, 00076 Aalto, Finland*

³⁾ *Materials Department, University of California, Santa Barbara, CA93106, USA*

^{a)}Electronic mail: dominik.zumbuhl@unibas.ch

The attenuation of a coaxial cable can be calculated by means of transmission line theory¹, which extends the description of discrete electronic components to distributed elements. For a coaxial cable with resistance R_{tot} [Ω/m], given by the sum of inner and outer conductor resistance R_{IC} and R_{OC} , with inductance L [H/m], capacitance C [F/m] and shunt conductance G [S/m] (note that all parameters are per length), the attenuation in units of decibel as a function of frequency ν reads:

$$\text{Attenuation}(\nu) = 20 \log |e^{-\gamma z}|, \quad \gamma = \sqrt{(R_{\text{tot}} + 2\pi i \nu L)(G + 2\pi i \nu C)} \quad (1)$$

Here, z denotes the wire length in units of m. Parameters R_{tot} , L , C and G may be calculated from geometric dimensions of the coaxial cable (inner conductor diameter D , thickness $d_{\text{Ins.}}$ of the polyurethane insulation and d_{epoxy} for the epoxy outer conductor), and material properties such as the dielectric constant $\epsilon_{\text{Ins.}}$ of the polyurethane insulation and the conductivity σ_{Cu} , σ_{epoxy} , $\sigma_{\text{Ins.}}$ of inner conductor, outer conductor and the insulator, respectively:

$$\begin{aligned} R_{\text{tot}} = R_{\text{IC}} + R_{\text{OC}} &= \frac{1}{\sigma_{\text{Cu}} \left(\frac{D}{2}\right)^2 \pi} + \frac{1}{\sigma_{\text{epoxy}} \left(\left(\frac{D}{2} + d_{\text{Ins.}} + d_{\text{epoxy}}\right)^2 - \left(\frac{D}{2} + d_{\text{Ins.}}\right)^2\right) \pi} \\ C &= \frac{2\pi\epsilon_0\epsilon_{\text{Ins.}}}{\ln\left(\frac{D/2 + d_{\text{Ins.}}}{D/2}\right)} \\ L &= \frac{\mu_{\text{Ins.}}}{2\pi} \ln\left(\frac{D/2 + d_{\text{Ins.}}}{D/2}\right) \\ G &= \frac{\sigma_{\text{Ins.}}}{\epsilon_{\text{Ins.}}} C \end{aligned} \quad (2)$$

As discussed in the main text, the skin effect forces AC currents to the conductor surface i.e. the skin depth $\delta_{\text{Cu}} = 1/\sqrt{\sigma_{\text{Cu}}\mu_{\text{Cu}}\nu\pi}$ in case of copper and $\delta_{\text{epoxy}} = 1/\sqrt{\sigma_{\text{epoxy}}\mu_{\text{epoxy}}\nu\pi}$ for the epoxy outer conductor (the permeabilities μ_{Cu} , μ_{epoxy} and $\mu_{\text{Ins.}}$ are assumed to be equal to the vacuum permeability μ_0 , since all those materials, copper and Ag-epoxy and polyurethane, are not magnetic). As a consequence, the resistance is modified to:

$$\begin{aligned} R_{\text{IC}}(\nu) &= \frac{1}{\sigma_{\text{Cu}} \cdot \left(\left(\frac{D}{2}\right)^2 - \left(\frac{D}{2} - \delta_1\right)^2\right)}, \quad \delta_1 = \min(\delta_{\text{Cu}}, D/2) \\ R_{\text{OC}}(\nu) &= \frac{1}{\sigma_{\text{epoxy}} \cdot \left(\left(\frac{D}{2} + d_{\text{Ins.}} + \delta_2\right)^2 - \left(\frac{D}{2} + d_{\text{Ins.}}\right)^2\right)}, \quad \delta_2 = \min(\delta_{\text{epoxy}}, d_{\text{epoxy}}) \end{aligned} \quad (3)$$

Note that eq. 3 gives an approxiated solution for $R_{\text{IC}}(\nu)$ that is, however, very close to the exact solution which can be expressed in terms of bessel functions.

Next, experimental results are compared with attenuation curves obtained from transmission line theory, i.e. using eq. 1 (C , L and G are calculated from eq. 2 and the frequency dependent resistance is given in eq. 3). Fig. S1 shows the measured attenuation profile for a microwave filter with $z = 1.51$ m of copper wire, a total DC resistance and capacitance of $R_0 = 3.36 \Omega$ and $C = 2.54$ nF, respectively. In contrast to the filters in the main text, here the wire is wound as a 6 cm long and thin single layer coil to suppress parasitic capacitive couplings (due to the single layer design interlayer couplings are absent).

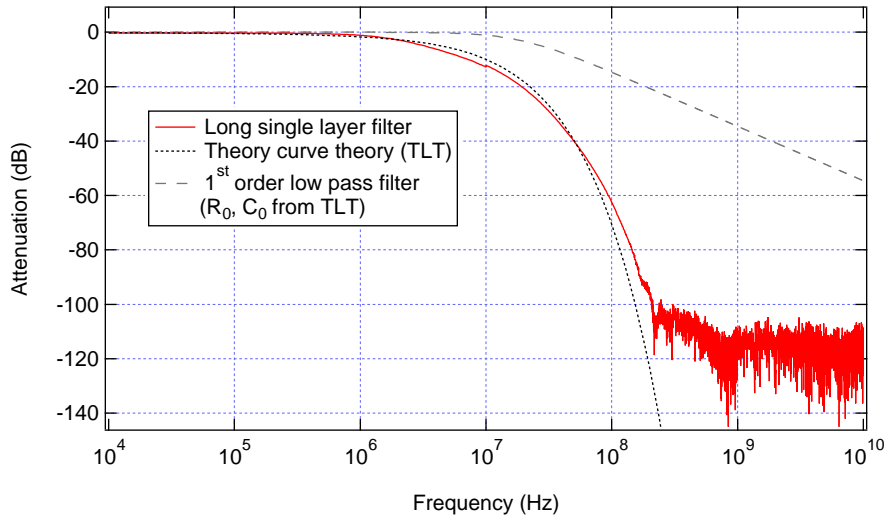


FIG. S1. Measured room temperature attenuation characteristics for a single layer microwave filter (no interlayer coupling) with $z = 1.51$ m of copper wire (red data). A theory curve using eq. 1 and the parameters from Tab. I, is shown as dotted, black curve. In dashed grey, a standard first order low-pass filter ($R_0 = R_{\text{tot}}z$ and $C_0 = Cz$ from theory curve) is shown for comparison.

The measured attenuation is in very good agreement with theoretical predictions for a 1.51 m long coax cable (black dashed line in Fig. S1) with inner and outer conductor made from copper and silver epoxy, respectively. We stress that the input parameters for the theory curve, given in Tab. I, arise from independently measured quantities and literature values that completely fix the attenuation profile without adjustable parameters. While the conductivity of copper σ_{Cu} , the thickness d_{epoxy} of the epoxy layer have a minor influence on the transmission profile (given the low conductivity $\sigma_{\text{Ins.}}$ of polyurethane, the shunt term is negligible), the other quantities affect it quite strongly.

We note that since R_{tot} is dominated by the outer conductor at high frequencies, a replace-

ment of the inner conductor with e.g. resistive wire, does not improve the filter performance, provided that the resistivity of the inner conductor stays well below that of silver epoxy. For the same reason, the transmission does not significantly alter at cryogenic temperatures, though the conductivity of the copper wire significantly increases (a residual resistance ratio of $RRR = 128$ was measured for the present wire, whereas $RRR \sim 3$ for the silver epoxy).

D	$97 \pm 2 \mu\text{m}$	measured ($D = 100 \mu\text{m}$ stated by the manufacturer ²)
$d_{\text{Ins.}}$	$8 \pm 2 \mu\text{m}$	measured
d_{epoxy}	$\approx 2 \text{ mm}$	cross section of the filter
z	1.51 m	measured
$\epsilon_{\text{Ins.}}$	4.6 ± 1	chosen to match the measured capacitance with the above wire dimensions
$\sigma_{\text{Ins.}}$	$< 9.3 \cdot 10^{-14} \text{ S/m}$	measured
σ_{Cu}	$5.95 \cdot 10^7 \text{ S/m}$	Ref. 4
σ_{epoxy}	$\geq 2 \cdot 10^5 \text{ S/m}$	Ref. 3

TABLE I. Material parameters and geometrical dimensions used for the theory curve shown in Fig. S1.

From eq. 2 the filter DC resistance $R_0 = (R_{\text{IC}}(\nu = 0) + R_{\text{OC}}(\nu = 0)) \cdot z \approx R_{\text{IC}}(\nu = 0) \cdot z$ can easily be calculated, $R_0 = 3.43 \pm 0.15 \Omega$, in good agreement with the measured resistance of 3.36Ω .

To emphasize the filter performance, the theoretical attenuation profile for a standart first order low-pass filter with $R_0 = 3.36 \Omega$ and $C_0 = 2.54 \text{ nF}$ is shown in fig. S1 (dashed grey) in addition to the data and transmission line model.

REFERENCES

¹David M. Pozar, Microwave Engineering, third edition, John Wiley & sons Inc. (2005)

²Insulated copper wire CUL 200/0.1, available at distrelec, www.distrelec.ch

³Datasheet for conductive silver epoxy E4110, available at EPO-TEK

⁴G. K. White and P. J. Meeson, Experimental techniques in low-temperature physics, Oxford University Press (2002).